Catal Lett (2012) 142:901–906
DOI 10.1007/s10562-012-0838-9

Hard Template Synthesis of Nanocrystalline $NaNbO_3$ with Enhanced Photocatalytic Performance

Xiukai Li · Zongjin Zhuang · Wei Li · Qing Li

Received: 19 March 2012 / Accepted: 25 April 2012 / Published online: 17 May 2012

Abstract A nanocasting method using SBA-15 as a hard template was adopted to prepare nanocrystalline $NaNbO_3$. The templated $NaNbO_3$ consists of single crystalline nanoparticles about 8 nm. The nanocrystalline $NaNbO_3$ sample showed remarkably enhanced photocatalytic activity for 2-propanol photodegradation in comparison to the counterpart prepared by the solid state reaction.

Keywords $NaNbO_3$ · Nanocrystalline · Alkalinity · Nanocasting · Photocatalysis

1 Introduction

The preparation of size controlled nanocrystals is a hot topic in the area of materials science. As many metal oxide nanocrystals show distinct catalytic properties from the bulk ones [1–4], the preparation of metal oxide catalysts with nanocrystallinity by low-cost and innovative methods is currently of great interest. Although a variety of metal oxide nanocrystals have been successfully prepared [5–8], the fabrication of low-dimensional nanocrystals for some particular metal oxides, especially some complex metal oxides, is still a scientific challenge. One major difficulty is that high temperature treatment is usually required for the crystallization of metal oxides, which inevitably leads to the sintering of the starting particles.

There are several liquid phase techniques such as sol–gel synthesis [9], hydrothermal synthesis [10], and microemulsion synthesis [11] have been developed to prepare metal oxide nanocrystals with the particle size ranging from 10 to 100 nm. However, the particles are usually poorly crystallized. Nanocasting technique with mesoporous materials as hard template provides an efficient method to prepare isolated nanocrystalline particles [1, 6, 12–16]. The well-ordered mesopores of siliceous material (e.g., SBA-15, KIT-6) or carbon can serve as the nano-reactor to accommodate the precursors of metal oxides. After the calcination treatment and removal of the template, the nanocrystals of metal oxide could be obtained. Because the nanocrystals of metal oxides are confined within the mesopores of the template, the uncontrolled growth of the particles could be avoided. In some cases the closely packed nanoparticles can also generate ordered interparticle mesoporosity [1, 6, 13–16]. Several transition-metal containing nanocrystalline metal oxides (e.g., MnO_2 [1], Co_3O_4 [13, 15], and $LaFeO_3$ [6]) have been successfully prepared by the nanocasting technique with mesoporous materials as the hard template. However, there has been no similar report about the preparation of alkali-metal containing metal oxides.

Perovskite structured $NaNbO_3$ has a variety of unique ferroelectric [17], optical [18, 19], and photocatalytic properties [20–23]. Extensive work has been devoted to prepare $NaNbO_3$ with various nanostructures [18, 19, 22–25]. However, most of the reported samples have particle size ranging from several tens of nanometer to micrometer. In this work, we purposely prepared nanocrystalline $NaNbO_3$ by the

X. Li · Z. Zhuang · W. Li · Q. Li
China–Australia Joint Research Center for Functional Molecular Materials, Jiangsu University, Zhenjiang 212013, People's Republic of China

X. Li (✉) · Z. Zhuang · W. Li · Q. Li
Scientific Research Academy, Jiangsu University, No. 301 Xuefu Road, Zhenjiang 212013, People's Republic of China
e-mail: li.xiukai@gmail.com

X. Li · Z. Zhuang · W. Li · Q. Li
School of Chemistry and Chemical Engineering, Jiangsu University, Zhenjiang 212013, People's Republic of China

nanocasting technique with SBA-15 as a template. Special attentions were paid to the alkalinity of the alkali metal on sample synthesis. The samples were characterized by XRD, N_2-sorption measurement, HRTEM, UVDRS, and Raman spectroscopy. The photocatalytic activities of the sample were evaluated for 2-propanol (isopropanol, IPA) photodegradation in gas phase.

2 Experimental

2.1 Sample Preparation

The SBA-15 template was prepared according to the well established liquid crystal template method according to the procedure described previously [26]. The precursors of $NaNbO_3$ were introduced to the mesopores of SBA-15 by the incipient wetness impregnation method. Sodium nitrate was used as Na source and niobium oxalate was used as Nb source, respectively; water was used as a solvent. The mass ratio of $NaNbO_3$ precursors to SBA-15 was 5:1. The impregnated SBA-15 was dried at 80 °C overnight. The sample was further calcined at 600 °C for 4 h for the crystallization of $NaNbO_3$. The silica template was removed by stirring the $NaNbO_3$/SBA-15 sample in NaOH solution (2 M) for 36 h. The NaOH solution was replaced every 12 h. The obtained $NaNbO_3$ was washed thoroughly with deionized water and then dried at 80 °C. The $NaNbO_3$ sample prepared by such hard template nanocasting method was designated as $NaNbO_3$(HT). In the solid state reaction synthesis, stoichiometric amounts of Nb_2O_5 and Na_2CO_3 were well milled, and then calcined at 900 °C for 24 h with interim grinding. The sample prepared by the solid state reaction was designated as $NaNbO_3$(SSR).

2.2 Sample Characterization

The phase compositions of samples were identified by X-ray Powder Diffraction (Cu Kα radiation, Bruker AXS-D8) in the 2θ range of 1–90°. The UV–Vis diffuse reflectance spectra were recorded at room temperature on a Shimadzu UV-2450 UV–Vis spectrometer with barium sulfate as the reference sample. Specific surface areas of samples were deduced by the BET method (N_2 adsorption) with a NOVA-2000E instrument. Morphologies of samples were characterized using a high resolution transmission electron microscope (HR JEM-2100, JEOL). EDS analysis was performed on a scanning electron microscope (JSM-7001F, JEOL). The Raman spectra were collected using a DXR Raman Spectrometer (Thermo Fisher) at room temperature with excitation source of 513 nm and power of 1.0 mW.

2.3 Activity Evaluation

The photocatalytic degradation of IPA was carried out in a quartz tubular reactor (length = 28.0 cm, $\varnothing$ = 3.0 cm; volume = 159 ml) that was placed horizontally. A flat quartz plate was used to hold the catalyst (typically 50 mg). The reactor was purged with dry synthetic air for more than 10 min after the sample was loaded. The reactor was sealed and then desired amount of IPA/air mixture was introduced by syringe. Prior to light irradiation, the reactor was left in the dark for at least 4 h until an adsorption–desorption equilibrium was finally established. A 350 W Xe-lamp (Nanshen Company, Shanghai) was used as light source. A water filter was also used to remove the light in the infrared region. The products in the gas phase were analyzed with a gas chromatograph system (GC-9790A), using a flame ionization detector for organic compounds determination.

3 Results and Discussion

Figure 1 shows the XRD patterns of the $NaNbO_3$ samples prepared by the hard template nanocasting technique. The sample prepared by the solid state reaction method was also shown for reference. The sodium to niobium ratio is crucial for the formation of pure phase $NaNbO_3$. In case stoichiometric amounts of Na and Nb precursors were used in sample synthesis, an impurity phase in addition to rhombohedral $NaNbO_3$ (JCPDS: 01-073-0803) was detected after the calcination treatment. Pure phase $NaNbO_3$ could be obtained by varying the Na/Nb molar ratio to 1.5. The diffraction intensities of the $NaNbO_3$ samples synthesized by the hard template method are much weaker than those of the sample prepared by the solid state reaction method, possibly because of the much smaller crystallite size of the $NaNbO_3$(HT) samples. It is likely that the alkali metal Na can react readily with silica to form sodium silicate species during the calcination treatment, thus at least 50 % excess of $NaNO_3$ should be added to compensate the loss of Na. We got similarly results in the preparation of $LiNbO_3$ and $KNbO_3$. Pure phase $LiNbO_3$ could be prepared when 50 % excess of $LiNO_3$ was used. However, as to the preparation of $KNbO_3$, the impurity phases were presented even when up to 100 % excess of KNO_3 or potassium oxalate was used. It is envisioned that since K has stronger alkalinity than Li and Na, the K ions can react more easily with the siliceous template accordingly.

The N_2-sorption isotherms of samples and their corresponding pore size distributions are illustrated in Fig. 2, with the related data given in Table 1. The $NaNbO_3$(HT) sample exhibited type IV isotherm with hysteresis loop (Fig. 2a), signifying mesoporous structure. The sudden increase in the

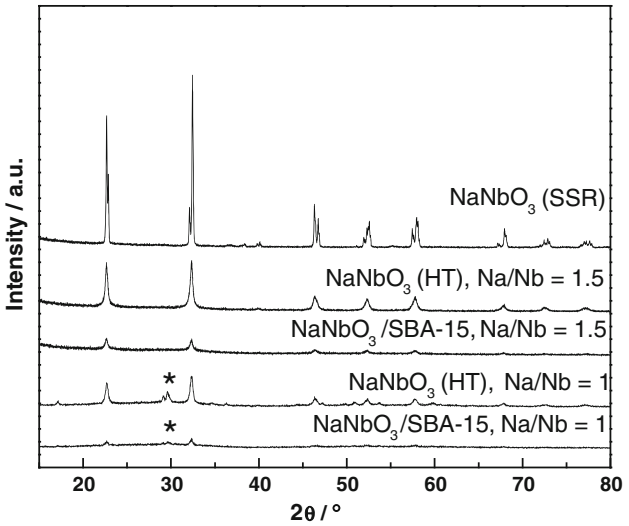

Fig. 1 XRD patterns of $NaNbO_3$ samples prepared by the solid state reaction (SSR) method and the hard template (HT) method. The *asterisk* indicates the impurity phase present in the samples

volume of gas uptake within the relative pressure (P/P_0) range of approximately 0.7–1.0 should be attributed to the capillary condensation of N_2. Figure 2b depicts the pore size distribution deduced from the desorption branch of the N_2-sorption isotherms. The $NaNbO_3$(HT) sample exhibited a rather broader pore size distribution, probably because the pore walls of the SBA-15 template were severely corroded by the alkaline sodium precursor. The specific surface area value of $NaNbO_3$(HT) was 32.2 $m^2\ g^{-1}$ (Table 1), the data is much greater than that (1.3 $m^2\ g^{-1}$) of $NaNbO_3$(SSR).

Transmission electron microscopy (TEM) was used to investigate the microstructure of samples. From Fig. 3a one can see that the $NaNbO_3$(HT) sample consists of isolated nanoparticles with diameter of about 8 nm. The value is close to the pore diameter (ca. 8.3 nm) of SBA-15. Thus it follows that $NaNbO_3$ was replicated fidelity from the mesopores of SBA-15 in the present work. The HRTEM images and the SAED patterns show that each particle of $NaNbO_3$(HT) belongs to a single crystal with high crystallinity. The lattice fringes could be indexed to the (100) spacing of $NaNbO_3$. It is likely that these closely packed nanoparticles generate weak interparticle mesoporosity. As such mesoporosity is interparticle porosity rather than intraparticle porosity, the long-range ordered mesoporous structure was not observed in the XRD measurement.

Figure 4 shows the UV–Vis absorption spectra of the templated sample. The spectrum of the sample prepared by the solid state reaction is also shown for comparison. $NaNbO_3$ is a wide band gap semiconductor [27] and absorbs light in the UV region of $\lambda < 380$ nm. The significant blue shift of the absorption edge was observed for the templated sample, and this is probably because of the quantum-size effect of the nanoparticles. The band gap

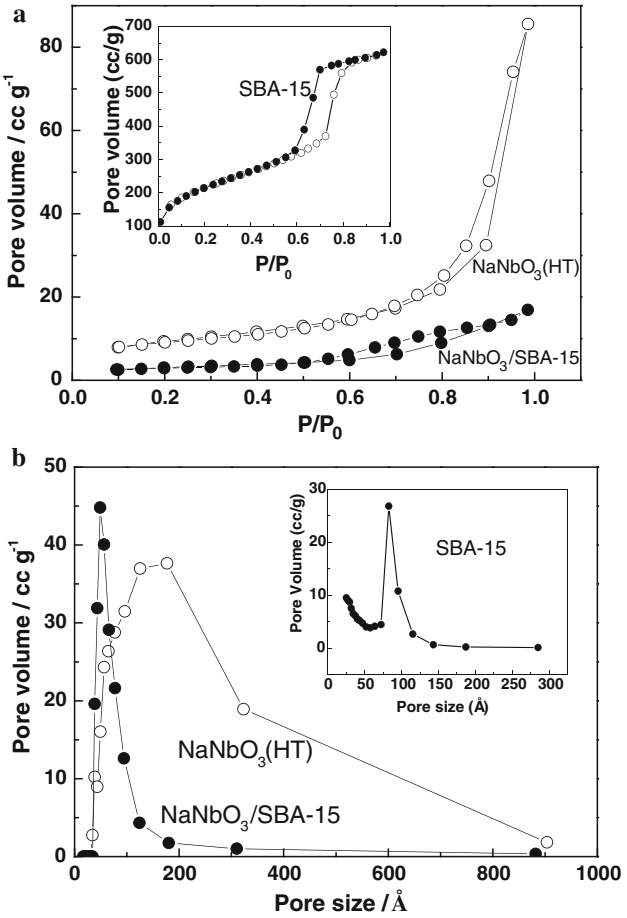

Fig. 2 The adsorption–desorption isotherms (**a**) and the pore size distributions (**b**) of $NaNbO_3$(HT) before and after the removal of the SBA-15 template. The data of the SBA-15 template was also shown in the *insets*

values were estimated from the sharp absorption edges of the spectra, and the data are given in Table 1. Compared with that of the sample prepared by the solid state reaction, the band gap value of $NaNbO_3$(HT) increased 0.3 eV.

Figure 5 shows the Raman spectra of the samples. The spectrum of $NaNbO_3$(SSR) are in good agreement with those reported in the literatures [28–32]. The peaks in the 100–300 cm^{-1} (v_1) and 500–700 cm^{-1} (v_2) regions could be assigned to the internal vibrations of the NbO_6 octahedra in the perovskite structure [29]. The weak bands appeared at 375–430 cm^{-1} (v_3) correspond to the associated bending modes of the Nb–O–Nb linkage [30]. Much weaker scattering peaks were recorded for the $NaNbO_3$ sample prepared by the nanocasting technique. The splitting of peaks in the regions of v_1 and v_2 bands disappeared. Such changes are attributed to the much smaller particle size of the templated sample [29].

The photocatalytic properties of $NaNbO_3$ samples were evaluated for IPA photodegradation in gas phase. IPA photodegradation usually proceeds via an acetone

Table 1 The physical characteristics of samples

Sample	BET surface area ($m^2\ g^{-1}$)	Pore diameter (nm)	Pore volume ($cm^3\ g^{-1}$)	Particle size (nm)	Bandgap (eV)
SBA-15	762.6	8.3	0.96	–	–
$NaNbO_3$(HT)	32.2	17.7	0.13	8[a]	3.7
$NaNbO_3$(SSR)	1.3	–	–	>1000[b]	3.4

[a] The data was estimated from the TEM image shown in Fig. 3

[b] The data was estimated from the SEM image

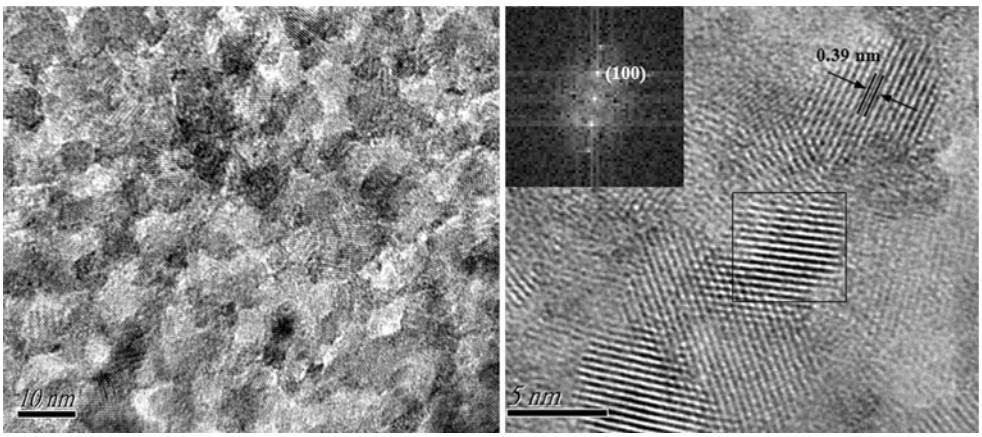

Fig. 3 TEM and HRTEM images of $NaNbO_3$(HT) that synthesized by the nanocasting technique

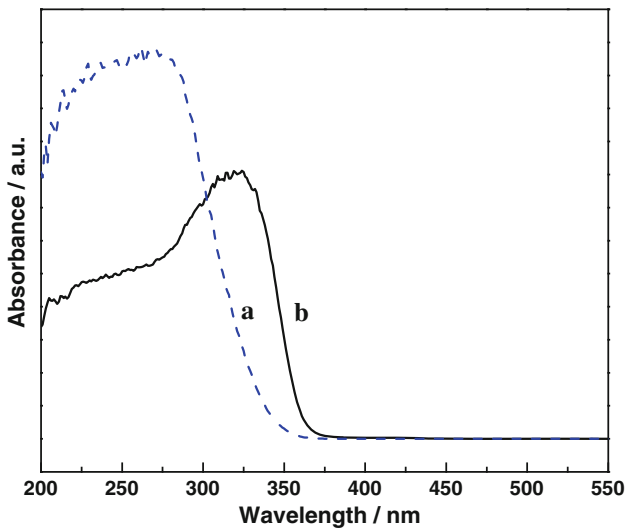

Fig. 4 The absorption spectra of (*a*) $NaNbO_3$(HT) and (*b*) $NaNbO_3$-(SSR)

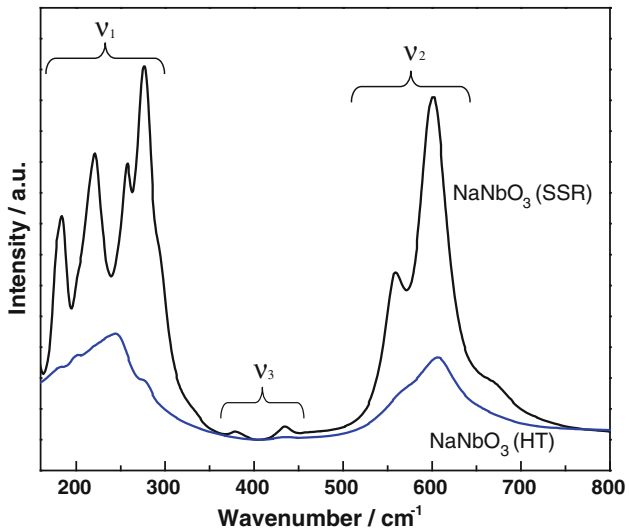

Fig. 5 Raman spectra of $NaNbO_3$ samples prepared by the solid state reaction method and the hard template nanocasting technique

route, that is, IPA is first photo-oxidatively dehydrogenated to acetone and eventually photo-oxidized to CO_2. Thus IPA photodegradation to acetone was usually taken as a model reaction to evaluate the photocatalytic activity of semiconductors [33–36]. Figure 6 shows the concentration of evolved acetone over the $NaNbO_3$ samples under UV light irradiation. Acetone was detected over all the samples when the light was turned on, while there was no acetone detected

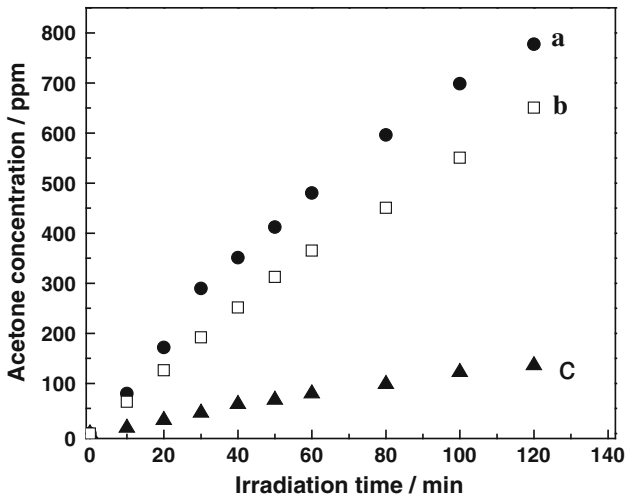

Fig. 6 The photocatalytic degradation of IPA to acetone over (*a*) $NaNbO_3$(HT, Na/Nb = 1.5), (*b*) $NaNbO_3$(HT, Na/Nb = 1), and (*c*) $NaNbO_3$(SSR). *Reaction conditions*: catalyst = 50 mg; irradiation intensity = 34.8 mW cm^{-2}. The initial concentration of IPA was about 1.0×10^4 ppm

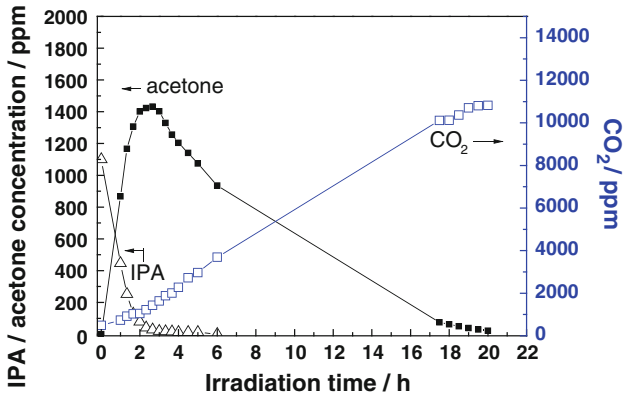

Fig. 7 The photocatalytic mineralization of IPA to carbon dioxide over $NaNbO_3$(HT, Na/Nb = 1.5). *Reaction conditions*: catalyst = 50 mg; irradiation intensity = 42.8 mW cm^{-2}. The initial concentration of IPA was about 8.0×10^3 ppm

under the dark condition or when the sample was absent. The samples prepared by the hard template method showed notably enhanced activity compared with the sample prepared by the solid state reaction. The rate of acetone evolution increased 8 times for $NaNbO_3$(HT, Na/Nb = 1.5). The activity of $NaNbO_3$(HT, Na/Nb = 1) is lower than that of $NaNbO_3$(HT, Na/Nb = 1.5), and this is probably because of the presence of the impurity phase in the former sample. Figure 7 shows the rate of CO_2 evolution over the $NaNbO_3$(HT, Na/Nb = 1.5) sample. One can see that CO_2 concentration increased linearly with irradiation time. Nearly 45 % of IPA was mineralized to CO_2 after 20 h of irradiation. It is apparent that the hard template synthesized $NaNbO_3$ has better photocatalytic performance. Since both the $NaNbO_3$(HT) and $NaNbO_3$(SSR) samples are crystallized in the same perovskite structure, we deduce that the higher surface area and the smaller particle size of $NaNbO_3$(HT) contribute to its higher catalytic activity. It was generally recognized that the separation and transportation of photogenerated carriers (i.e., electrons and holes) is crucial for the photocatalytic activity. As the sample prepared by the hard template method consists of nanoparticles while the sample prepared by the solid state reaction consists of micron-sized particles, the photogenerated carriers in $NaNbO_3$(HT) could migrate to the surface of the sample more quickly than in the $NaNbO_3$(SSR) case. The larger surface area usually means more active sites per unit mass of sample, which may also contribute to the higher catalytic activity of the catalyst. Our experiments show that the $NaNbO_3$(HT) sample showed 10 % greater amount of IPA adsorption than the $NaNbO_3$(SSR) sample under the dark condition. In view of the fact that the uptake of IPA increased only 10 % while the photocatalytic activity enhanced 8 times, we conclude that the efficiency of carries transportation and separation determined mainly by the particle size should be the primary factor that contribute to the remarkably enhanced photocatalytic activity of $NaNbO_3$(HT).

4 Conclusion

Hard template nanocasting technique was adopted to prepare nanocrystalline $NaNbO_3$. The alkalinity of sodium has profound impacts on sample synthesis. The alkali metal ions can react easily with the siliceous template, and this affects the formation of pure phase $NaNbO_3$. At least 50 % excess of Na precursor should be used to prepare pure phase $NaNbO_3$. The TEM investigations revealed that the $NaNbO_3$(HT) sample consists of isolated particles with particle size of ca. 8 nm. These closely packed nanoparticles generate interparticle mesoporosity. The HRTEM images and the SAED patterns show that each particle of $NaNbO_3$(HT) belongs to a single crystal with high crystallinity. Appreciable blue shift of the absorption edge was observed for the templated $NaNbO_3$(HT) sample. The Raman response of the $NaNbO_3$ sample is sensitive to the particle size. The $NaNbO_3$(HT) sample showed notably enhanced activity for IPA photodegradation in gas phase.

Acknowledgments This research was supported by the National Natural Science Foundation of China (No. 21003064), the Research Foundation of Jiangsu University (No. 09JDG042), and the Scientific Research Foundation for the Returned Overseas Chinese Scholars, State Education Ministry.

References

1. Jiao F, Bruce PG (2007) Adv Mater 19:657
2. Heer S, Lehmann O, Haase M, Gudel HUB (2003) Angew Chem Int Ed 42:3179
3. Rossinyol E, Prim A, Pellicer E, Arbiol J, Hernández-Ramírez F, Peiró F, Cornet A, Morante JR, Solovyov LA, Tian B, Bo T, Zhao D (2007) Adv Funct Mater 17:1801
4. Balasubramanian B, Kraemer KL, Reding NA, Skomski R, Ducharme S, Sellmyer DJ (2010) ACS Nano 4:1893
5. Wang X, Zhuang J, Peng Q, Li Y (2005) Nature 437:121
6. Valdes-Solis T, Marban G, Fuertes AB (2005) Chem Mater 17:1919
7. Mialon G, Gohin M, Gacoin T, Boilot JP (2008) ACS Nano 2:2505
8. Tang J, Redl F, Zhu Y, Siegrist T, Brus LE, Steigerwald MT (2005) Nano Lett 5:543
9. Pasricha R, Ravi V (2005) Mater Lett 59:2146
10. Liu JF, Li XL, Li YD (2003) J Cryst Growth 247:419
11. Adityawarman D, Voigt A, Veit P, Sundmacher K (2005) Chem Eng Sci 60:3373
12. Zhu K, He H, Xie S, Zhang X, Zhou W, Jin S, Yue B (2003) Chem Phys Lett 377:317
13. Yue W, Hill AH, Harrison A, Zhou W (2007) Chem Commun 24:2518
14. Li G, Zhang D, Yu JC (2008) Chem Mater 20:3983
15. Wang Y, Yang C, Schmidt W, Spliethoff B, Bill E, Schuth F (2005) Adv Mater 17:53
16. Shi Y, Wan Y, Liu R, Tu B, Zhao D (2007) J Am Chem Soc 129:9522
17. Du HL, Tang FS, Liu DJ, Zhu DM, Zhou WC, Qu SB (2007) Mater Sci Eng B 136:165
18. Lu CH, Lo SY, Lin HC (1998) Mater Lett 34:172
19. Dutto F, Raillon C, Schenk K, Radenovic A (2011) Nano Lett 11:2517
20. Shi H, Li X, Iwai H, Zou Z, Ye J (2009) J Phys Chem Solids 70:931
21. Li G, Yang N, Wang W, Zhang WF (2009) J Phys Chem C 113:14829
22. Lv J, Kako T, Li Z, Zou Z, Ye J (2010) J Phys Chem C 114:6157
23. Shi H, Li X, Wang D, Yuan Y, Zou Z, Ye J (2009) Catal Lett 132:205
24. Song H, Ma W (2011) Ceram Inter 37:877
25. Zhu HY, Zheng ZF, Gao XP, Huang YN, Yan ZM, Zou J, Yin HM, Zou QD, Kable SH, Zhao JC, Xi YF, Martens WN, Frost RL (2006) J Am Chem Soc 128:2373
26. Zhao D, Feng J, Huo Q, Melosh N, Fredrickson GH, Chmelka BF, Stucky GD (1998) Science 279:548
27. Kenji S, Kazunori K, Akihiko K (2011) Dalton Trans 40:3909
28. Jehng J, Wachs I (1991) Chem Mater 3:100
29. Shiratori Y, Magrez A, Dornseiffer J, Haegel F, Pithan C, Waser R (2005) J Phys Chem B 109:20122
30. Li G, Kako T, Wang D, Zou Z, Ye J (2007) J Solid State Chem 180:2845
31. An C, Tang K, Wang C, Shen G, Jin Y, Qian Y (2002) Mater Res Bull 37:1791
32. Camargo ER, Kakihana M (2001) Chem Mater 13:1905
33. Ohko Y, Hashimoto K, Fujishima A (1997) J Phys Chem A 101:8057
34. Xu W, Raftery D, Francisco JS (2003) J Phys Chem B 107:4537
35. Xu W, Raftery D (2001) J Phys Chem B 105:4343
36. Larson SA, Widegren JA, Falconer JL (1995) J Catal 157:611